Dalton Transactions

ROYAL SOCIETY OF CHEMISTRY

PAPER

View Article Online
View Journal | View Issue

Cite this: *Dalton Trans.*, 2025, **54**, 11878

An imidazolium dication affords a stable UWY-like zeolite and enables a subtle structure direction towards EMM-17†

Huajian Yu,[a,b] Peng Lu,‡[a] Zihao Rei Gao, *§[a] Alvaro Blanco[a] and Miguel A. Camblor *[a]

Zeolites with interconnected medium (10Ring) and large (12R) pores, such as the **UWY** framework type, hold significant potential for catalysis but may suffer from instability due to a high germanium content required for their synthesis. Addressing this limitation, we report the synthesis of HPM-9, a novel **UWY**-like germanosilicate zeolite, utilizing 1,1′-(1,8-octanediyl)bis(3-methylimidazolium) (8BMI) as the organic structure-directing agent (OSDA) in fluoride media. HPM-9 achieves significantly lower germanium content (Ge_f = Ge/(Ge + Si) down to 0.14) compared to the original IM-20 (Ge_f = 0.3), resulting in markedly improved stability upon calcination and exposure to water. Structural analysis using synchrotron powder X-ray diffraction (SPXRD) suggested disorder and DIFFaX simulations revealed that HPM-9 exhibits minimal stacking faults along the *a*-axis, corresponding to an intergrowth with a polymorph where double four-membered rings (*d4r*) are partially replaced by single four-membered rings (*s4r*), likely driven by the reduced Ge content. Furthermore, decreasing the Ge content further ($Ge_f \leq 0.05$) subtly shifts the structure direction towards EMM-17, a zeolite featuring interconnected 11R and 10R pores. ^{19}F MAS NMR suggests the presence of *d4r* units in the synthesized EMM-17, and we propose a mechanism where the less stable *d4r*-containing polymorph C nucleates first, templating the subsequent growth of *d4r*-free polymorphs A and B by epitaxial intergrowth. Comparative studies with analogous OSDAs (7BMI and 9BMI) confirmed the optimal linker length of 8BMI for directing towards stable **UWY** structures. The enhanced stability of HPM-9 opens avenues for the practical application of **UWY**-type zeolites in catalysis.

Received 16th June 2025,
Accepted 12th July 2025

DOI: 10.1039/d5dt01413a

rsc.li/dalton

Introduction

Zeolites, with their varied complex frameworks and widely diverse applications, have been at the forefront of research in materials science and catalysis for decades. The possibility to fine-tune properties for specific applications has driven the ongoing quest for new zeolite topologies and compositions.[1] One of the key factors influencing zeolite performance is the size and dimensionality of their pores. Medium pore zeolites, characterized by rings of 10 tetrahedra (10R) as minimum apertures along the diffusion path, typically exhibit shape selectivity, which is crucial in catalytic reactions where specific molecular sizes and shapes need to be accommodated and/or diffuse. In contrast, large pore zeolites with 12-membered rings (12R) facilitate enhanced molecular diffusion, allowing for the processing of larger molecules. Zeolites that combine intersecting medium and large pores have garnered significant interest due to their potential to offer a unique combination of reactivity, selectivity, and stability.[2]

The **UWY** zeolite framework type,[3] whose reference material is zeolite IM-20,[4] is a prime example of such a zeolite. It features intersecting 12R and 10R pores, making it an attractive candidate for various catalytic applications. For instance, a hypothetical Ge-free aluminosilicate **UWY** zeolite has been proposed as a potential catalyst for the transalkylation of trimethylbenzene with toluene.[5] However, despite its potential there has been little further research on the synthesis and applications of IM-20. The original synthesis of IM-20 involves a relatively high germanium content (Ge_f = Ge/(Ge + Si) = 0.4 in the gel, 0.3 in the product), which compromises its stability.

[a]*Instituto de Ciencia de Materiales de Madrid (ICMM), CSIC, 28049 Madrid, Spain. E-mail: macamblor@icmm.csic.es*
[b]*Escuela de Doctorado, Universidad Autónoma de Madrid, Madrid 28049, Spain*
†Electronic supplementary information (ESI) available. See DOI: https://doi.org/10.1039/d5dt01413a
‡Present address: The ZeoMat Group, Qingdao Institute of Bioenergy and Bioprocess Technology, Chinese Academy of Sciences, 266101 Qingdao, China.
§Present address: Department of Chemical and Biomolecular Engineering and Institute for NanoBioTechnology, Johns Hopkins University, Baltimore, MD, USA. E-mail: zgao44@jhu.edu

A newer report on the synthesis of this type of zeolite as nanosheets did not advance from this point of view, while demonstrated both the potential of the material for biomass conversion and the low stability issue.[6] The **UWY** topology contains abundant double four-membered rings (*d4r*), known to be strained for pure silica compositions. Such structures are generally only accessible by increasing the flexibility of the SiO_2 framework by introducing fluoride in the synthesis, with fluoride lowering the covalent character of the Si–O bond and being trapped inside the *d4r*.[7,8] Alternatively, or simultaneously, introduction of Ge helps stabilizing *d4r* structures due to the sharper T–O–T angles and longer T–O bonds upon isomorphous substitution of Si by Ge as a tetrahedral T atom.[9] Thus, the potential applicability of **UWY** zeolites demands new synthesis routes that can produce stable **UWY** zeolites with low Ge content capable of withstanding calcination and exposure to ambient conditions without degradation.

This study addresses this challenge through the synthesis of HPM-9, a novel **UWY**-like zeolite with a significantly lower germanium content (Ge_f down to 0.14) and an improved stability upon calcination and exposure to water. Interestingly, the organic structure-directing agent (OSDA) used in its synthesis, 1,1′-(1,8-octanediyl)bis(3-methylimidazolium) (8BMI), is formally a dimer of the one reported for IM-20 (1-butyl-3-methylimidazolium) (Scheme 1).

Additionally, we found a subtle but very interesting structure-direction effect under certain conditions at an even lower Ge_f in the gel, which lead to the formation of EMM-17, a zeolite with interconnected large 11R and medium 10R pores.[10] A mechanistic hypothesis, based on the existence of polymorph C, is proposed to explain this.

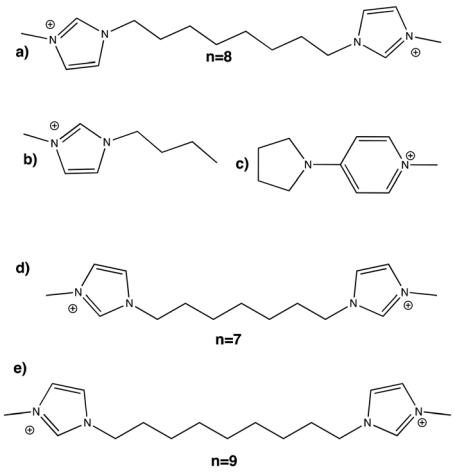

Scheme 1 Five OSDAs relevant to this work: (a) 8BMI [1,1′-(1,8-octanediyl) bis(3-methylimidazolium)] used to synthesize stable HPM-9 (**UWY**), (b) 1-butyl-3-methylimidazolium used in the original synthesis of IM-20 (**UWY**) in ref. 4. (c) 1-Methyl-4-(pyrrolidinyl)pyridinium used for the discovery of aluminosilicate EMM-17 in ref. 10, and two OSDA's related to 8BMI used here for comparison (d) 7BMI [1,1′-(1,7-heptanediyl)bis(3-methylimidazolium)], (e) 9BMI [1,1′-(1,9-nonanediyl)bis(3-methylimidazolium)].

Experimental

OSDA synthesis

8BMI: 12.316 g (150 mmol, 2eq.) 1-methylimidazole (Fluorochem, 99%) was added with 250 mL acetonitrile (Scharlau, HPLC grade) into a flask under magnetic stirring. After 20.402 g (75 mmol, 1 eq.) 1,8-dibromooctane (Aldrich, 98%) was added, the system was refluxed for 4d. The crude product was collected by evaporating the solvent and it was purified by dissolving in water followed by washing with diethyl ether (100 ml × 3). The purity of 8BMI dibromide salt was determined by LNMR in DMSO-d_6 (^{1}H NMR (300 MHz): δ 9.35 (s, 2H), 7.89 (s, 2H), 7.78 (s, 2H), 4.18 (t, 4H), 3.80 (s, 6H), 1.67 (m, 4H), 1.08 (m, 8H); ^{13}C NMR (75 MHz): δ136.64, 123.74, 122.57, 49.16, 36.49, 29.75, 28.35, 25.57). Using the same procedure but adding 1,7-dibromoheptane (Aldrich, 95%) and 1,9-dibromononane (Aldrich, 98%) instead of 1,8-dibromooctane we obtained 7BMI and 9BMI, respectively. 7BMI, DMSO-d_6, 300 MHz, ^{1}H NMR: δ 9.42 (s, 2H), 7.95 (s, 2H), 7.83 (s, 2H), 4.18 (t, 4H), 3.87 (s, 6H), 1.66 (m, 4H), 1.04 (m, 6H); ^{13}C NMR (75 MHz): δ 136.73, 123.72, 122.54, 49.06, 36.53, 29.63, 27.84, 25.41. 9BMI, DMSO-d_6, 300 MHz, ^{1}H NMR: δ 9.52 (s, 2H), 7.98 (s, 2H), 7.87(s, 2H), 4.20 (t, 4H), 3.89 (s, 6H), 1.72 (m, 4H), 1.13 (m, 10H); ^{13}C NMR (75 MHz): δ136.88, 123.84, 122.66, 49.09, 36.38, 29.85, 28.92, 28.59, 25.76.

Anion exchange

35 mmol 8BMIBr (7BMIBr, 9BMIBr) was dissolved in deionized water with 140 mL resin (hydroxide form, Amberlite IRN78, 1.1 meq mL^{-1} by wetted bed volume) under stirring overnight. The solution was filtered and the resin washed with deionized water (until neutral). The obtained solution was then concentrated by evaporation and the final concentration of OSDA $(OH)_2$ was determined by titration of OH^- with 0.1261 M HCl (aq.)

Zeolite synthesis

Stable HPM-9 was discovered by high-throughput experiments involving 8BMI, fluoride and Ge by varying Ge_f, OH/T, H_2O/T, OH/F, temperature, and crystallization time. Pure HPM-9 was obtained in a synthetic gel with a composition of 0.25 OSDA $(OH)_2$: 0.5HF : 0.1GeO_2 : 0.9 SiO_2 : 10H_2O heated at 160 °C for 7 days. When Ge_f decreased to 0.05 and 0.025, EMM-17 was obtained as main phase with trace amount impurities from a gel with composition of 0.25 OSDA$(OH)_2$: 0.5HF : 0.05 or 0.025 GeO_2 : 0.95 or 0.975 SiO_2 : 10H_2O heated at 160 °C for 12 days. The detailed synthesis results of all the experiments are listed in Tables S1 and S2.†

In a typical synthesis, GeO_2 was dissolved in 8BMI$(OH)_2$ ([OH^-] = 0.2344 mmol g^{-1}) and stirred few hours until the solution became clear. Then, TEOS was added to the solution and the mixture was stirred overnight for hydrolysis while all the ethanol and some water were allowed to evaporate. Subsequently, HF was added into the mixture, then the beaker was placed into a 90 °C oven for evaporating excess water. When the weight of the beaker reached the targeted amount,

the mixture was stirred by hand to make it as homogeneous as possible before putting it into an autoclave. The autoclave was placed at 160 °C in a static oven for 7 d (or 12 d for EMM-17). After that, the product was collected by filtration and washed with deionized water and acetone.

Characterization

Laboratory powder X-ray diffraction (PXRD, Bruker D8 Advance diffractometer, Cu Kα, λ = 1.5418 Å) was used to identify the zeolite phases. For better data quality, we collected synchrotron PXRD datasets (SPXRD) at the Spanish synchrotron light source (ALBA, Cerdanyola del Vallès, Barcelona, BL04-MSPD) in capillary mode. CHN elemental analysis of as-made zeolites was measured on a LECO CHNS-932 analyzer. Thermogravimetric and differential thermal analyses (TG-DTA) were performed on a TA SDT Q600 thermal analyzer, 10 °C min^{-1} up to 1000 °C, 100 mL min^{-1} air. FE-SEM (Field-emission electron microscopy) and EDS (Energy Dispersive Spectroscopy, Genesis XM2i detector) were used to check zeolite morphology and determine its Ge_f on a FEI Nova NanoSEM 230 microscope. Liquid nuclear magnetic resonance (LNMR, ^{1}H and ^{13}C) spectra were obtained on a Bruker Avance III-HD Nanobay 300 MHz and a Bruker 300 MHz. Multinuclear (^{1}H, ^{13}C, ^{19}F and ^{29}Si) solid-state magic angle spinning (MAS) spectra were acquired on Bruker AV-400-WB equipment and the detailed experimental conditions have been reported elsewhere.[8] The Ar adsorption isotherm was obtained at 87 K in a Quantachrome Autosorb iQ.

Rietveld refinement of a calcined HPM-9 with a measured Ge_f = 0.2 (0.15 in the synthesis mixture) was performed against SPXRD data (λ = 0.49587 Å) using the GSAS-II suite.[11] The starting model was obtained from IZA-SC[3] by assuming Ge atoms (Ge_f = 0.2, 12 Ge per uc) are distributed evenly in 10 T atoms. 22 coefficients were used to fit the background with a Chebyschev-1 function. A pseudo-Voigt function (U, V, W, X, Y), uniaxial size model and generalized microstrain model were used for peak-shape fitting before the structure refinement. Sample displacement to beam and unit cell were varied during Rietveld refinement. 40 bond soft restraints (T–O:1.68 Å) and 88 angle soft restraints (O–T–O: 109.54°, T–O–T: 145°) were applied. Several constraints were used including that Si and Ge atoms in the same T atoms site have the same coordinates, the sum of their occupancies were constrained to 1, all O, Si and Ge atoms have same displacement parameter and there were a total of 12 Ge atoms per unit cell. After peak-shape fitting and atom coordinate refinement, the occupancies of T atoms and displacement parameters were refined and the occupancy of Ge was fixed to 0 if it became negative during refinement.

Results and discussion

HPM-9 synthesis and characterization

Tables S1 and S2† list the synthesis results. In the absence of Ge (Table S1†), the synthesis with or without Al is dominated by **MFI** type zeolites (and/or **MFI-MEL** intergrowths), a default zeolite not demanding of a strong structure-direction effect. Experiments with Ge were then performed (Table S2†), using a lower temperature to favour less dense phases. Most experiments were done in static conditions to overcome the limited number of rotation sites in our ovens. Using Ge we first discovered HPM-9, later recognized as a zeolite with **UWY** topology. The Ge_f of HPM-9 is typically slightly larger than that in the synthesis mixture for low Ge_f and slightly lower for high Ge_f, while at a Ge_f of 0.3 both values are similar. Interestingly, we were able to get HPM-9 at Ge_f values much lower than those reported for IM-20, the reference material for this topology.[4,6] While IM-20 had a reported Ge_f = 0.3 (0.4 in the gel) and after calcination requires storage under dry conditions to prevent degradation,[4] HPM-9 with a Ge_f of 0.14 determined by EDS (0.1 in the gel) can withstand calcination and exposure to ambient air without structural degradation, making it a more viable candidate for industrial applications (Fig. 1). The measured BET area of HPM-9 is 445 m^2 g^{-1}. The calcined zeolite is also stable after immersion in water for one hour.

UWY contains a large number of *d4r* (two crystallographically different *d4r* amounting to 3 *d4r* per unit cell of 60 T, with 24 T sites belonging to *d4r*), known to be favored by both F and Ge.[7,9,12,13] The ^{19}F MAS NMR spectra of three HPM-9 samples with Ge_f = 0.14, 0.31 and 0.41 show only resonances in the 0 to −40 ppm chemical shift range, corresponding to F occluded in *d4r*. For a Ge_f of 0.14 (8.4 Ge per uc) the spectrum contains three resonances at −40, −21 and −10 ppm, corresponding to F anions occluded in *d4r* of types I, II and III, respectively.[14] Their relative intensities are approximately 1 : 4 : 6, respectively. If there were a 100% preference of Ge for T sites in *d4r* and Ge were equally distributed among the *d4r*, then an average of 2.8 Ge per *d4r* could be calculated (0.14 × 60/3). For a random distribution of Ge among all T sites the average would be 1.1 Ge per *d4r* (24 × 0.14/3). Since resonance

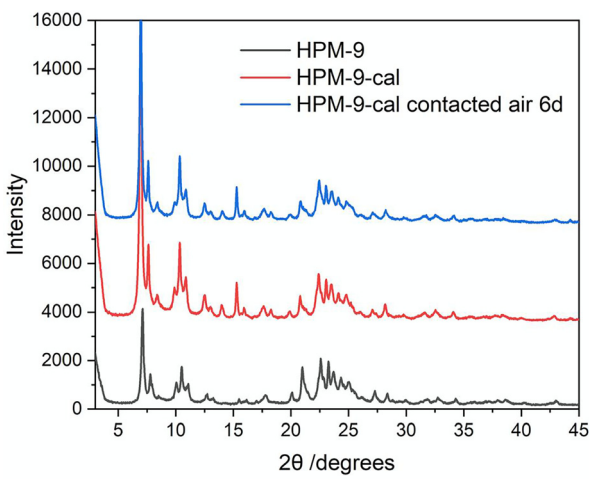

Fig. 1 PXRD of (from bottom) HPM-9 as-made, calcined and calcined and exposed to ambient air for 6 days. By contrast, HPM-9 with higher Ge_f significantly degraded upon calcination and air exposure (Fig. S1†).

I corresponds to F in *d4r* with no Ge, its presence in this HPM-9 with Ge_f = 0.14 suggests the distribution of Ge among T sites but also among *d4r* is not random (Fig. 2) and demonstrate the existence of a non-negligible content of pure silica *d4r* in this HPM-9 (around 10% if all *d4r* are occupied by fluoride). Additionally, this suggests Ge pairing are somehow favored at that Ge_f because site type III (Ge pairs with no more than 2 Ge neighbors) occurs while there are still *d4r* with a low Ge content (type II, non-paired Ge) or no Ge at all (type I, no Ge). On the contrary, when the Ge_f is increased to 0.3 in the gel (0.31 in the zeolite, 18.6 Ge per uc) and 0.5 (0.41 in the zeolite, 24.6 Ge per uc), resonances I and II disappear and only resonance III (implying between two and six Ge per *d4r*) is observed. Resonance III is symmetric in both samples and can be fitted with a single Gaussian peak. This is also the resonance reported in the original IM-20 (−8.9 ppm, attributed in that report to Ge in a *d4r* containing five Ge).[4] For a Ge_f = 0.41, the number of Ge atoms per unit cell (24.6) already surpasses the number of available T sites in *d4r* (24) and, despite that fact, resonance IV (at least one Ge with at least 3 Ge neighbors) is still not present (it should appear at a chemical shift between those of resonances II and III, at around −14 ppm). Hence, these results suggest there may be a tendency to avoid extensive Ge pairing in **UWY** even at relatively high loadings. An avoidance of Ge pairing has been proposed in **AST** only for Ge_f < 0.5,[15] while it was discarded in **STW**, where Ge pairings appeared even at very low Ge_f below 0.1.[14] This suggests Ge pairing in zeolites might be highly structure dependent. The fact that we observe a tendency to pairing at low Ge_f (0.14) and a tendency to avoid pairings at high Ge_f may indicate that the preference of Ge for sites in *d4r* is not very strong in **UWY**. A caveat about this conclusion is that resonances III and IV might perhaps appear in **UWY** at chemical shifts too close to distinguish between them. The general observations discussed above (a tendency of Ge to cluster at low Ge_f and a topology-dependent clustering) appear to agree with the conclusions of a recent analysis of the Ge distribution in zeolites using neural network potentials.[16]

The morphology of the HPM-9 crystals varies along with variations of Ge_f and water/T ratio in the gel. HPM-9 tends to crystallize in the form of round hollow aggregates composed of small plaques randomly interpenetrated (Ge_f = 0.1, water/T = 10, Fig. 3b). However, upon dilution (Ge_f = 0.1, water/T = 15), interpenetrated larger plaques are formed instead (Fig. 3c). At high Ge_f very small needles are formed (Fig. 3d) while we have also obtained "house of cards" aggregates at very low Ge_f (Ge_f = 0.05, water/T = 10, Fig. 3a). The corresponding PXRD patterns are shown in Fig. S2.†

The ^{13}C MAS NMR spectrum of as-made HPM-9 matches well with the liquid NMR spectrum of the OSDA (Fig. S3†), indicating the OSDA is intact after the synthesis. This was also proved by CHN element analysis, where the C/N ratio of the as-synthesized HPM-9 (4.0, Table 1) matches well with the calculated C/N ratio of the OSDA ($C_{16}N_4H_{28}$, C/N = 4). Organics and fluoride can be removed by calcination, most of it between 250 and 450 °C (Fig. S4†) in an exothermic process (Fig. S5†).

We then performed ^{29}Si direct polarization (DP) and $^{29}Si\{^1H\}$ cross polarization (CP) MAS NMR measurements on both the as-made and calcined HPM-9 (Ge_f = 0.14). For the as-made HPM-9, its DP spectrum possess a broad, featureless resonance ranging from −100 to −120 ppm (Fig. 4a). Because of the existence of Ge in tetrahedral framework positions, the resonances of neighboring Si shift to lower field, which is common in germanosilicate zeolites. The $^{29}Si\{^1H\}$ CP spec-

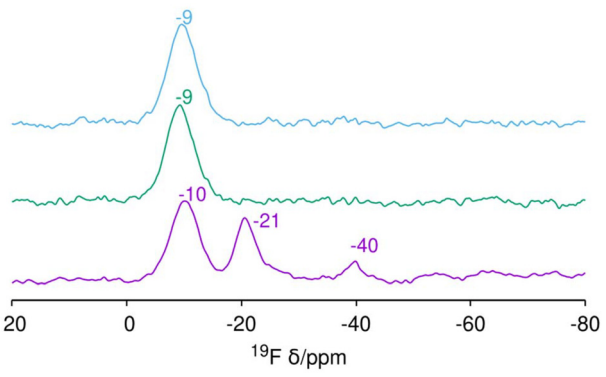

Fig. 2 ^{19}F MAS NMR spectra of HPM-9 with (from bottom to top) Ge_f = 0.14, Ge_f = 0.31, and Ge_f = 0.41. Chemical shifts of the resonances are marked. Peaks at −9/−10 ppm, −21 ppm, and −40 ppm correspond to resonances type III, II, and I, respectively, of the F anion occluded in *d4r*.[14]

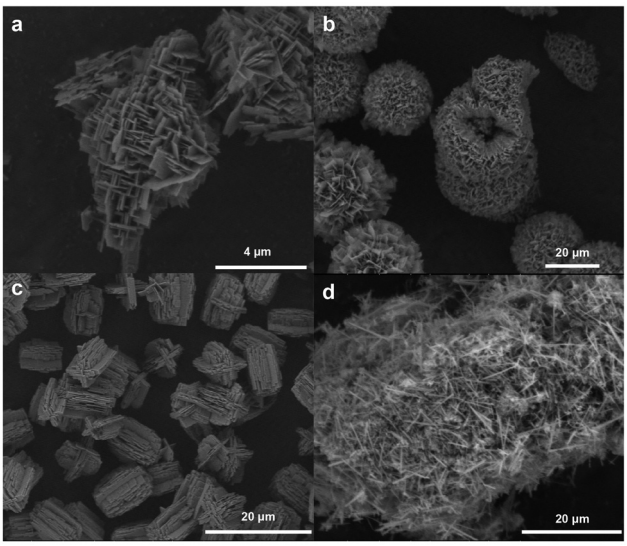

Fig. 3 The very different morphologies observed in the synthesized HPM-9 at 160 °C (OSDA/T = F/T = 0.5) as a function of the Ge_f and/or water/T ratio in the gel: (a) house of cards (under rotation with Ge_f = 0.05, water/T = 10; the sample contains traces of **MFI** and/or **TON** not observed here), (b) hollow spherical aggregates of thin plaques (static, Ge_f = 0.1, water/T = 10), (c) much thicker interpenetrated plaques by dilution (static, Ge_f = 0.1, water/T = 15, contains traces of **TON**), and (d) needles (as in b but increasing the Ge_f to 0.3; a further increase to Ge_f = 0.5 gives similar crystals).

Table 1 Chemical composition of HPM-9 and EMM-17

Phase	wt%			Molar ratios[a]		wt%[b]	
	N	C	H	C/N	H/N	TG residue	Unit cell[a]
HPM-9 Ge_f 0.14	2.66	9.06	1.50	3.97	7.85	82.9(83.6)	$(C_{16}N_4H_{28}(F,OH)_2)_{2.26}(H_2O)_{3.84}[Si_{51.6}Ge_{8.4}O_{120}]$
EMM-17 Ge_f 0.045	2.85	10.04	1.78	4.11	8.74	82.54(80.8)	$(C_{16}N_4H_{28}(F,OH)_2)_{4.71}(H_2O)_{16.19}[Si_{114}Ge_6O_{240}]$

[a] The C/N and H/N values for the 8BMI dication are 4 and 7, respectively. [b] The expected value according to the composition in the last column is written within parenthesis. The organic content of these materials continuously decreases upon washing suggesting strong adsorption in the outer surface.

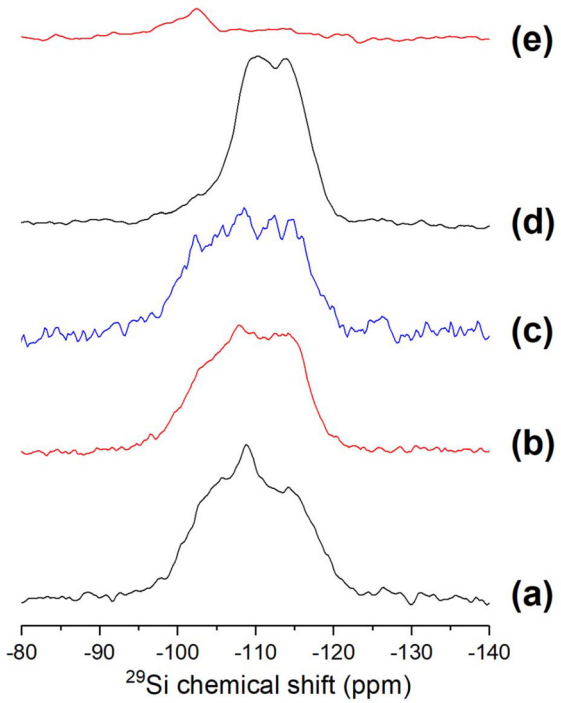

Fig. 4 ^{29}Si MAS NMR study of HPM-9: ^{29}Si direct polarization (DP) spectrum of as-made HPM-9 (a), $^{29}Si\{^1H\}$ cross-polarization (CP) spectra of as-made HPM-9 with long (6 ms) (b) and short (0.5 ms) contact time (c), ^{29}Si DP spectrum of calcined HPM-9 (d), and $^{29}Si\{^1H\}$ CP spectrum of calcined HPM-9 with 6 ms contact time (e). Numbers of scans for spectra (a–e): 952, 1024, 8192, 965, 2048 runs, respectively. Relaxation delays for spectra (a–e): 60, 5, 5, 60, 5 seconds, respectively.

trum with short contact time (0.5 ms) and longer scanning (8192 runs accumulation because of the poor intensity at short contact time, Fig. 4c) indicates at least five resonances in the range of −110 ppm to −120 ppm, plus another resonance at around −126 ppm, assigned to penta-coordinated Si in $\underline{Si}(OT)_4F$.[17] The possible existence of Q^3 sites, *i.e.* $\underline{Si}(OSi)_3(OH)$, cannot be ascertained because most H is contributed by the OSDA itself in the as-made zeolite sample. After calcination, the ^{29}Si DP spectrum possess three resonances, a small broad hump at −102 ppm, plus two stronger overlapped resonances at −110 ppm and −114 ppm (Fig. 4d). The one at −102 ppm was proved to be Q^3 sites by the CP spectrum (Fig. 4e) while the other two are Q^4 sites, where it is not possible to discern individual $\underline{Si}(OSi)_4$ and $\underline{Si}(OGe)(OSi)_3$ species. Considering the spectrum (e) in Fig. 4, the Q^3 site concentration must be very low in the calcined HPM-9, suggesting a good integrity after calcination of the zeolite with low Ge content, in agreement with PXRD results (Fig. 1).

Structural analysis of calcined HPM-9

After Rietveld refinement of HPM-9 against SPXRD data the refined Ge distribution basically agree with our conclusions from MAS NMR (*vide supra*). The two crystallographically different *d4r* have the same Ge content (2.4 Ge per *d4r*, amounting to 7.2 Ge) and there are 4.8 additional atoms dispersed in 4 T atoms outside *d4r*, supporting the idea that there is a tendency to avoid Ge pairings in **UWY**. Three sites outside *d4r* (sites T4, T7 and T8) have no Ge. However, the overall refinement failed to produce a completely satisfactory fit. While the numerical indicators (R_{wp} = 7.38%, GoF = 2.65) were relatively good, the Rietveld plot (Fig. 5) was indicative of problems in the structural model.[18] A detailed analysis showed that most of the peaks were broad, while (0, *k*, *l*) reflections were significantly sharper and this could not be adequately modeled by using anisotropic peak broadening strategies in GSAS-II. Additionally, the difference trace in Fig. 5 revealed that the position of the Bragg reflections were not consistently precise along the full profile. These observations suggested the

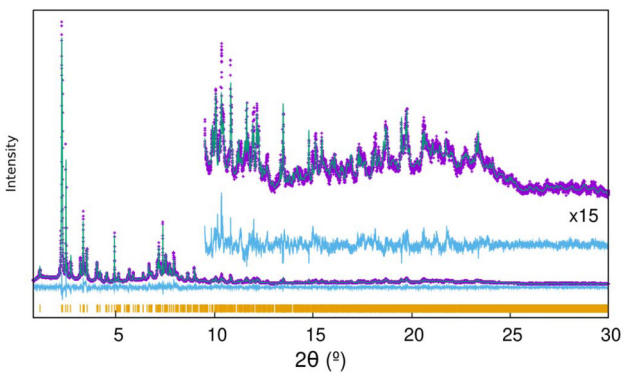

Fig. 5 Observed (purple +) and calculated (green solid line) synchrotron powder X-ray diffractograms for calcined HPM-9 refined in space group *Pmmm*. Vertical marks indicate the positions of allowed reflections. The cyan trace is the difference plot. The high angle region is also shown with expanded intensity (15×). λ = 0.49587 Å.

presence of stacking faults along the *a* direction. Examination of the **UWY** framework type revealed a possible stacking fault scheme where *d4r* along these direction were occasionally converted into single 4 rings (*s4r*) (Fig. 6). This would result in modulations of the *a* parameter that could account for the observations. This problem was tackled using DIFFaX, a program that calculates diffraction intensities from crystals faulted in one direction.[19] First, a fully ordered zeolite in which the concerned *d4r* were converted to *s4r* was built (Fig. 6). The resulting framework (polymorph B of HPM-9) contains medium 10R pores along the three crystallographic directions and was found to be topologically identical to the proposed polymorph A of zeolite ECNU-13, a disordered material that was very recently reported and whose synthesis makes use of the "monomer" 1-butyl-3-methylimidazolium.[20]

The coincidence of both framework types (polymorph A of ECNU-13 and polymorph B of HPM-9) has been confirmed by analysis of their coordination sequences using Kriber.[21] Then, both **UWY** and the new ordered zeolite were reoriented to have the stacking direction along *c* and DIFFaX files were constructed to simulate random intergrowths of both frameworks. The patterns obtained for different stacking probabilities (implying different proportions of both polymorphs) are depicted in Fig. S6,† where we can observe that at both extremes the simulated patterns agree well with the patterns of the ordered polymorphs simulated with VESTA software.[22] At intermediate probabilities the patterns are as expected: (0, *k*, *l*) reflections (Miller indexes according to the **UWY** orientation in the IZA database)[4] are much sharper and are unaffected in position by the probability of intergrowth, while any other reflection moves to higher 2θ angles and becomes broader as the proportion of the polymorph A of ECNU-13 increases. As shown in Fig. 7, the experimental pattern for HPM-9 agrees well with a disordered intergrown material with a very high proportion of **UWY** (estimated as around 95%). Given the stabilizing role that Ge exerts on *d4r*, the appearance of the kind of intergrowth observed, which imply a decrease in *d4r* units, is very likely a consequence of the decrease in the Ge_f.

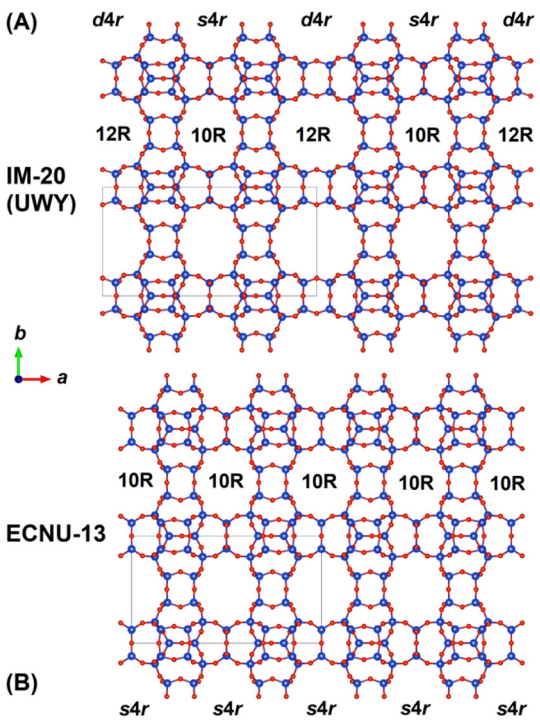

Fig. 6 The structures of **UWY** (A) and polymorph B (ECNU-13)(B) of the HPM-9 structure.

EMM-17 synthesis and characterization

Under certain conditions at very low Ge_f in the gel (0.05 and 0.025) we obtained zeolite EMM-17 (see Fig. S8†). This zeolite, which has interesting catalytic potential and also contains large (11R) and medium (10R) pore intersections,[10] is one of the rare "odd zeolites", *i.e.* those containing odd-membered pores.[23] In our syntheses EMM-17 frequently appears with trace impurities of zeolite **TON** or **MFI**. This structure-direction effect toward EMM-17 at very low Ge contents is intriguing because while Ge is known to structure-direct towards structures containing *d4r*, the reported EMM-17 topology is an intergrowth of two dominant polymorphs (A and B) that are devoid of such units. A third polymorph containing *d4r* units, polymorph C, was first proposed as hypothetical and later suggested to exist very minoritarily by high resolution electron microscopy.[24] The structure of the three polymorphs of EMM-17 are compared in Fig. S7.† Notably, the ^{19}F MAS NMR spectroscopy in Fig. 8 reveals the presence of a small but significant concentration of *d4r* in our EMM-17 zeolite (resonances I and II at −39 and −20 ppm, respectively) indirectly but strongly suggesting the existence of the less stable polymorph C (**MFI** and **TON** appearing as impurities, often at trace levels, don't contain *d4r*). This discovery enables us to propose, at a hypothetical level, a mechanistic explanation for the observed structure-direction effect: presumably, F (and Ge) initially help the nucleation of the less stable *d4r*-containing polymorph C, while this phase promotes in turn the subsequent formation of polymorphs A and B by epitaxial inter-

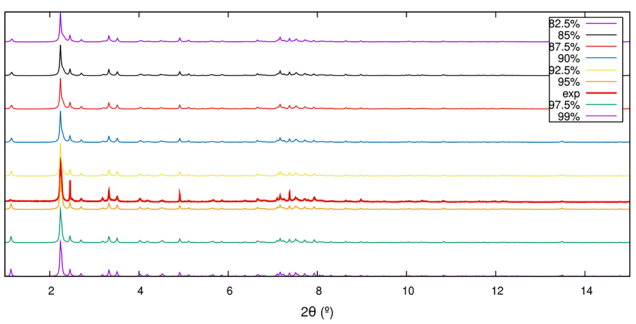

Fig. 7 DIFFaX simulated XRD patterns (λ = 0.49587 Å) for **UWY**-ECNU-13A intergrowths at high **UWY** proportions (thin traces, from bottom to top the **UWY** content is 99, 97.5, 95, 92.5, 90, 87.5, 85 and 82.5%). The thick red trace corresponds to the experimental SPXRD. For the whole **UWY**-ECNU-13A range, please check Fig. S6.†

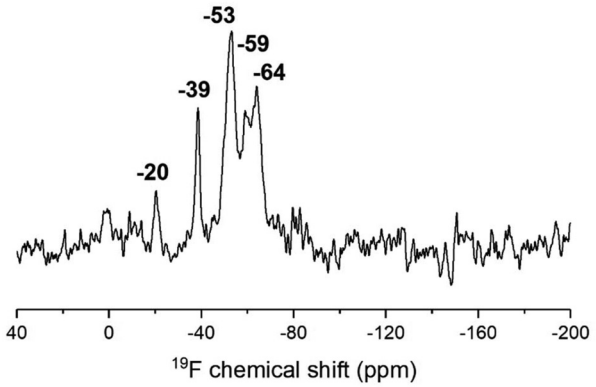

Fig. 8 ^{19}F MAS NMR spectrum of as-made EMM-17 using 8BMI as the OSDA at Ge_f 0.025. Resonances at −20 and −39 ppm correspond to types II and I, respectively, of F anions within *d4r* units while resonances at −53, −59, and −64 ppm are assigned to F anions confined within [$4^3 5^4$] cages.

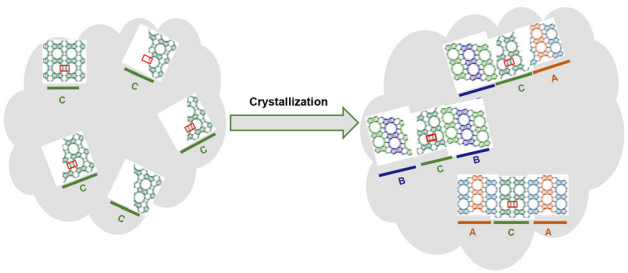

Fig. 9 Proposed mechanism for the crystallization of EMM-17 in this work. The presence of Ge and mostly F favours the nucleation of polymorph C of EMM-17 (left) which then grew to EMM-17 disordered materials by epitaxial intergrowth.

growth (Fig. 9).[25] The Ge_f of EMM-17 measured by EDS is a bit larger in the zeolite (0.045) than in the gel (0.025).

The much larger intensity of the resonance of type I compared to type II suggests the main *d4r* promoting effect is exerted by fluoride rather than Ge. However, when the Ge_f is decreased or increased, other phases (**MFI** and **TON** or HPM-9, respectively) compete. The high field signals observed in Fig. 8 at −53, −59 and −64 ppm can be unambiguously attributed to fluoride occluded in the [$4^3 5^4$] cage present in the three EMM-17 polymorphs,[26] although the −64 ppm resonance could also have a very minor contribution of F occluded in the [$4^1 5^2 6^2$] cage in trace **MFI**.[27] Resonances in similar chemical shift ranges are consistently attributed to F in [$4^3 5^4$] cages in several zeolites, including Beta (−58, −65, −70 ppm), **STT** (−56, −69 ppm) or **IFR** (−68 ppm).

At Ge_f = 0.025 our EMM-17 crystallizes in the form of very thin interpenetrated flakes giving the overall shape of a grain of rice, which we call "rice of cards" by analogy to the house of cards terminology (Fig. 10a and b). That morphology is markedly different from the reported ones,[10,24] with thicker plates that may interpenetrate without giving the regular overall morphology observed in our material. At a Ge_f = 0.05 our EMM-17 has the form of very small flakes aggregated in formations reminiscent of desert roses (Fig. 10c and d).

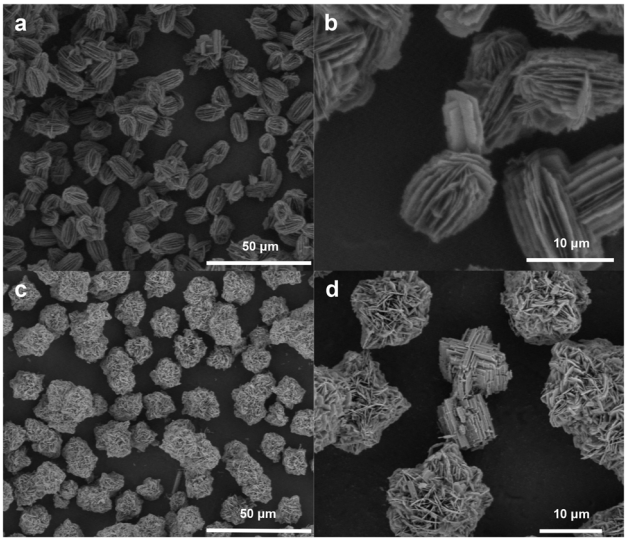

Fig. 10 Two typical morphologies found for EMM-17 synthesized using 8BMI: the rice of cards obtained at Ge_f = 0.025 (a and b) and the desert roses crystallized at Ge_f = 0.05 (c and d). In d, a **TON** impurity (as suggested by PXRD) is also observed.

Ill-crystallized phases and ITT

Both EMM-17 and HPM-9 appear to crystallize better at low concentrations (relatively high water/T ratios). In Table S2† several phases are listed as ill-crystallized (IC), although it is likely that the ill-defined PXRD patterns are just a consequence of a very small crystal size in the nanometer range. We have identified three different types of IC phases, ICa to ICc. PXRD of representatives of each IC group are shown in Fig. S9† and representative SEM images are shown in Fig. S10.† ICa are most likely nanosized HPM-9 and/or EMM-17. This is not only supported by the PXRD patterns but also from the infrared spectra in the region of framework vibrations, which may sometimes reveal the crystalline nature of nanophases better than the PXRD, as was clearly shown for instance in the case of nanozeolite Beta.[28] As shown in Fig. S11,† the spectra of all the ill-crystallized materials are rather similar and suggestive of crystalline zeolitic materials containing organic material, specially when compared with the IR spectrum of EMM-17. These ill-crystallized or nanosized phases are more frequent at low water contents and/or high Ge_f, suggesting nucleation under those conditions is fast while crystal growth is comparatively slow.

At a Ge_f of 0.5 and above a well-crystallized germanosilicate **ITT** zeolite starts to compete for crystallization.[29] This zeolite contains interconnected extra-large (18R) and medium (10R) pores and its well crystallized nature is evident in the PXRD pattern (Fig. S12†) and FESEM images (Fig. S13†) revealing small, submicrometer, hexagonal crystals.

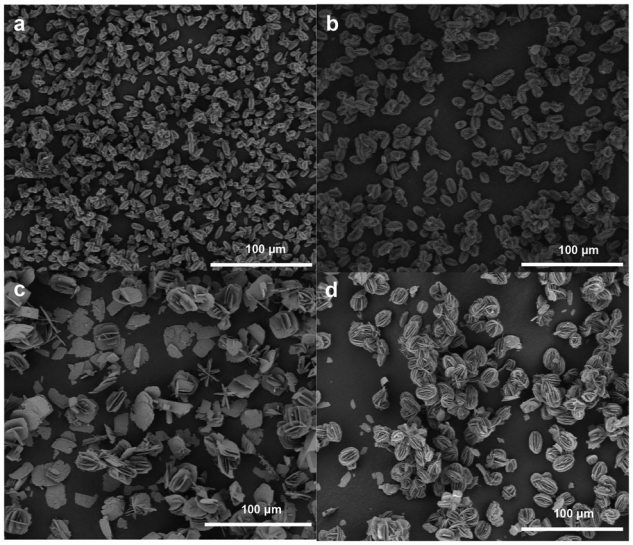

Fig. 11 FESEM images of EMM-17 obtained at Ge_f = 0.025 and water/T = 10 with 7BMI (a) and 8BMI (b) at 7d and with 9BMI at 7d (c) and 12d (d).

Comparison with 7BMI and 9BMI

As stated above, 8BMI is formally a dimer of the original OSDA for IM-20.[4] We have explored the use of two similar OSDAs with the imidazolium moieties separated by slightly shorter and longer linkers, *i.e.* with 7 and 9 methylene linkers (7BMI and 9BMI, respectively, in Table S2,† see Scheme 1) to check the importance of the linker's length. Although the structure direction of both was rather similar to that of 8BMI, the latter had a stronger effect towards HPM-9, exemplified by the fact that we were able to get pure HPM-9 with 8BMI at Ge_f = 0.1, while 7BMI and 9BMI produced mixtures with EMM-17. Moreover, at certain conditions producing pure HPM-9 with 8BMI (Ge_f = 0.5, water/T = 10), both the shorter and longer OSDAs produced a phase with a very low crystallinity (ICb) with traces of **ITT**. At a lower Ge_f (0.025) both 7BMI and 9BMI afforded EMM-17 (with trace impurities). The morphology for the 7BMI product at 7d was the noted rice of cards, while for 9BMI was an undeveloped rice of cards at 7d that finally evolved to the rice of cards at 12 days without an increase in the overall size of the particles. The particle size of the zeolite obtained with 7BMI was smaller than that of the zeolite prepared with 8BMI and much smaller than those prepared with 9BMI (Fig. 11).

Conclusions

A bisimidazolium dication, which is formally a dimer of the OSDA reported in the discovery of IM-20, affords the synthesis of HPM-9, a **UWY** type of zeolite with a significantly decreased Ge content. This endows the zeolite with a much higher stability upon calcination and exposure to water than the original **UWY** had. The improved stability may open the way to applications of this mixed large pore/medium pore (12R/10R) zeolite. OSDAs with slightly shorter or longer size have a poorer structure direction towards HPM-9. At least for the HPM-9 zeolite with low Ge content some disorder is observed, which can be conclusively attributed to the presence of stacking faults along the *a* axis. Even if the disorder can be considered minimal (around 95% is **UWY**), the faults are related to the conversion of some *d4r* into *s4r*, which can in turn be attributed to the decreased amount of Ge available to stabilize *d4r*.

At even lower Ge contents another mixed pore system (11R/10R) with the structure of EMM-17 was obtained. This is in spite of the lack of *d4r* in the predominant A and B polymorphs reported for this zeolite. ^{19}F MAS NMR reveals *d4r* do exist in our synthesized EMM-17 and we propose fluoride and, marginally, the small amount of Ge favors the formation of polymorph C, which contains *d4r*, and then polymorphs A and B grow by epitaxial intergrowth over polymorph C.

Author contributions

ZRG and MAC supervised the project, HY, PL and ZRG performed synthesis and characterization, AB and MAC worked on the DIFFaX simulations. MAC wrote the manuscript with input from all the authors.

Conflicts of interest

There are no conflicts to declare.

Data availability

Data for this article, including PXRD, SPXRD, DIFFaX simulated PXRD and multinuclear MAS NMR are available at DIGITAL.CSIC at **https://hdl.handle.net/10261/390152**.

Acknowledgements

Financial support from the Spanish Ministry of Science and Innovation (PID2022-137889OB-I00, MCIN/AEI/10.13039/501100011033) is gratefully acknowledged. Synchrotron powder X-ray diffraction data experiments were performed at the MSPD (Materials Science Powder Diffraction) beamline bl04 at the ALBA Spanish Synchrotron with the collaboration of the ALBA staff, and we gratefully thank Dr Alexander Missyul. H. Y. and P. L. are grateful to the China Scholarship Council for a PhD grant and a joint PhD research, respectively. P. L. acknowledges the support by Qingdao New Energy Shandong Laboratory of International Cooperation Project (QNESL ICP 202305).

References

1 H. Yu, L. A. Villaescusa, Z. R. Gao and M. A. Camblor, Stable Silica–Based Zeolites with Three–Dimensional Systems of Extra–Large Pores, *Angew. Chem., Int. Ed.*, 2024, **63**, e202412170.
2 R. F. Lobo and M. E. Davis, CIT-1: A New Molecular Sieve with Intersecting Pores Bounded by 10- and 12-Rings, *J. Am. Chem. Soc.*, 2002, **117**, 3766–3779.
3 C. Baerlocher and L. B. McCusker, Database of Zeolite Structures, **https://www.iza-structure.org/databases/**, (accessed May 12th, 2025).
4 M. Dodin, J.-L. Paillaud, Y. Lorgouilloux, P. Caullet, E. Elkaïm and N. Bats, A Zeolitic Material with a Three-Dimensional Pore System Formed by Straight 12- and 10-Ring Channels Synthesized with an Imidazolium Derivative as Structure-Directing Agent, *J. Am. Chem. Soc.*, 2010, **132**, 10221–10223.
5 J. Toda and G. Sastre, Diffusion of Trimethylbenzenes, Toluene, and Xylenes in UWY Zeolite as a Catalyst for Transalkylation of Trimethylbenzenes with Toluene, *J. Phys. Chem. C*, 2018, **122**, 7885–7897.
6 J. Wang, X. Ren, Q. Xiang, J. Jiang, F. Wang, Y. Guan, H. Xu and P. Wu, Double Unit-Cell Silicogermanate Nanosheets Developed by Salting-Out Mechanism for Biomass Conversion, *J. Am. Chem. Soc.*, 2024, **146**, 18418–18426.
7 C. M. Zicovich-Wilson, M. L. San-Román, M. A. Camblor, F. Pascale and J. S. Durand-Niconoff, Structure, Vibrational Analysis, and Insights into Host–Guest Interactions in As-Synthesized Pure Silica ITQ-12 Zeolite by Periodic B3LYP Calculations, *J. Am. Chem. Soc.*, 2007, **129**, 11512–11523.
8 A. Rojas, E. Martínez-Morales, C. M. Zicovich-Wilson and M. A. Camblor, Zeolite Synthesis in Fluoride Media: Structure Direction toward ITW by Small Methylimidazolium Cations, *J. Am. Chem. Soc.*, 2012, **134**, 2255–2263.
9 T. Blasco, A. Corma, M. J. Díaz-Cabañas, F. Rey, J. A. Vidal-Moya and C. M. Zicovich-Wilson, Preferential Location of Ge in the Double Four-Membered Ring Units of ITQ-7 Zeolite, *J. Phys. Chem. B*, 2002, **106**, 2634–2642.
10 S. C. Weston, B. K. Peterson, J. E. Gatt, W. W. Lonergan, H. B. Vroman, M. Afeworki, G. J. Kennedy, D. L. Dorset, M. D. Shannon and K. G. Strohmaier, EMM-17, a New Three-Dimensional Zeolite with Unique 11-Ring Channels and Superior Catalytic Isomerization Performance, *J. Am. Chem. Soc.*, 2019, **141**, 15910–15920.
11 B. H. Toby and R. B. Dreele, GSAS-II: the genesis of a modern open-source all purpose crystallography software package, *J. Appl. Crystallogr.*, 2013, **46**, 544–549.
12 S. Valencia, PhD Thesis, Universidad Politécnica de Valencia, 1997.
13 J.-L. Paillaud, Y. Lorgouilloux, B. Harbuzaru, P. Caullet, J. Patarin and N. Bats, presented in part at the From Zeolites to Porous MOF Materials – The 40th Anniversary of International Zeolite Conference, 2007.
14 R. T. Rigo, S. R. G. Balestra, S. Hamad, R. Bueno-Perez, A. R. Ruiz-Salvador, S. Calero and M. A. Camblor, The Si–Ge substitutional series in the chiral STW zeolite structure type, *J. Mater. Chem. A*, 2018, **6**, 15110–15122.
15 Y. Wang, J. Song and H. Gies, The substitution of germanium for silicon in AST-type zeolite, *Solid State Sci.*, 2003, **5**, 1421–1433.
16 I. Saha, A. Erlebach, P. Nachtigall, C. J. Heard and L. Grajciar, Germanium Distributions in Zeolites Derived from Neural Network Potentials, *Catal. Sci. Technol.*, 2024, **14**(20), 5838–5853.
17 H. Koller, A. Wölker, L. A. Villaescusa, M. J. Díaz-Cabañas, S. Valencia and M. A. Camblor, Five-Coordinate Silicon in High-Silica Zeolites, *J. Am. Chem. Soc.*, 1999, **121**, 3368–3376.
18 B. H. Toby, R factors in Rietveld analysis: How good is good enough?, *Powder Diffr.*, 2006, **21**, 67–70.
19 M. M. J. Treacy, J. M. Newsam and M. W. Deem, A general recursion method for calculating diffracted intensities from crystals containing planar faults, *Proc. R. Soc. London, Ser. A*, 1991, **433**, 499–520.
20 M. Peng, Q. Deng, Y. Zhao, H. Xu, Y. Guan, J. Jiang, L. Han and P. Wu, ECNU–13: A High–Silica Zeolite with Three–Dimensional and High–Connectivity Multi–Pore Structures for Selective Alkene Cracking, *Angew. Chem., Int. Ed.*, 2023, **62**, e202217004.
21 R. Bialek, *Kriber 1.2*, 2010.
22 K. Momma and F. Izumi, VESTA3 for three-dimensional visualization of crystal, volumetric and morphology data, *J. Appl. Crystallogr.*, 2011, **44**, 1272–1276.
23 M. A. Camblor, M.-J. Díaz-Cabañas, J. Perez-Pariente, S. J. Teat, W. Clegg, I. J. Shannon, P. Lightfoot, P. A. Wright and R. E. Morris, SSZ–23: An Odd Zeolite with Pore Openings of Seven and Nine Tetrahedral Atoms, *Angew. Chem., Int. Ed.*, 1998, **37**, 2122–2126.
24 X. Liu, L. Liu, T. Pan, N. Yan, X. Dong, Y. Li, L. Chen, P. Tian, Y. Han, P. Guo and Z. Liu, The Complex Crystal Structure and Abundant Local Defects of Zeolite EMM–17 Unraveled by Combined Electron Crystallography and Microscopy, *Angew. Chem., Int. Ed.*, 2021, **60**, 24227–24233.
25 S. Nair, M. Tsapatsis, L. A. Villaescusa and M. A. Camblor, Zeolite-β grown epitaxially on SSZ-31 nanofibers, *Chem. Commun.*, 1999, 921–922.
26 M. A. Camblor, P. A. Barrett, M. A.-J. Díaz-Cabañas, L. A. Villaescusa, M. Puche, T. Boix, E. Pérez and H. Koller, High silica zeolites with three-dimensional systems of large pore channels, *Microporous Mesoporous Mater.*, 2001, **48**, 11–22.
27 P. Lu, L. Gómez-Hortigüela and M. A. Camblor, Synthesis of pure silica MFI zeolites using imidazolium-based long dications. A comparative study of structure-directing effects derived from a further spacer length increase, *Dalton Trans.*, 2018, **47**, 7498–7504.
28 Synthesis of nanocrystalline zeolite beta in the absence of alkali metal cations, in *Stud. Surf. Sci. Catal*, ed. M. A. Camblor, A. Corma, A. Mifsud, J. Pérez-Pariente and S. Valencia, 1997.
29 A. Corma, M. J. Díaz-Cabañas, J. L. Jordá, C. Martínez and M. Moliner, High-throughput synthesis and catalytic properties of a molecular sieve with 18- and 10-member rings, *Nature*, 2006, **443**, 842–845.